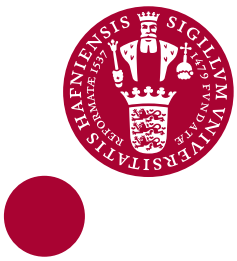

The source of inorganic nitrogen has distinct effects on cell wall composition in Brachypodium distachyon

Gazowska, Sylwia; Baldwin, Laetitia; Mravec, Jozef; Bukh, Christian; Fangel, Jonathan U.; Willats, William Gt; Schjoerring, Jan K.

Published in:
Journal of Experimental Botany

DOI:
10.1093/jxb/erz388

Publication date:
2019

Document version
Publisher's PDF, also known as Version of record

Journal of Experimental Botany, Vol. 70, No. 21 pp. 6461–6473, 2019
doi:10.1093/jxb/erz388 Advance Access Publication August 24, 2019
This paper is available online free of all access charges (see https://academic.oup.com/jxb/pages/openaccess for further details)

RESEARCH PAPER

The source of inorganic nitrogen has distinct effects on cell wall composition in *Brachypodium distachyon*

Sylwia Głazowska, Laetitia Baldwin, Jozef Mravec, Christian Bukh, Jonathan U. Fangel, William G.T. Willats and Jan K. Schjoerring*

Department of Plant and Environmental Sciences, University of Copenhagen, Thorvaldsensvej 40, DK-1871 Frederiksberg C, Denmark

* Correspondence: jks@plen.ku.dk

Received 21 March 2019; Editorial decision 16 August 2019; Accepted 19 August 2019

Editor: Qiao Zhao, Tsinghua University, China

Abstract

Plants have evolved different strategies to utilize various forms of nitrogen (N) from the environment. While regulation of plant growth and development in response to application of inorganic N forms has been characterized, our knowledge about the effect on cell wall structure and composition is quite limited. In this study, we analysed cell walls of *Brachypodium distachyon* supplied with three types of inorganic N (NH_4NO_3, NO_3^-, or NH_4^+). Cell wall profiles showed distinct alterations in both the quantity and structures of individual polymers. Nitrate stimulated cellulose, but inhibited lignin deposition at the heading growth stage. On the other hand, ammonium supply resulted in higher concentration of mixed linkage glucans. In addition, the chemical structure of pectins and hemicelluloses was strongly influenced by the form of N. Supply of only NO_3^- led to alteration in xylan substitution and to lower esterification of homogalacturonan. We conclude that the physiological response to absorption of different inorganic N forms includes pleotropic remodelling of type II cell walls.

Keywords: Ammonium, arabinoxylans, *Brachypodium distachyon*, cellulose, cell wall, ferulic acid, homogalacturonan, lignin, mixed linkage glucan, nitrate.

Introduction

Nitrogen (N) is an essential element for plant growth and development. Plants are able to absorb both organic (amino acids and peptides) and inorganic (ammonium and nitrate) N pools present in the soil (Näsholm *et al.*, 2009; Bloom, 2015). Some plants favour one of the N sources over others, often reflecting an adaptation to certain specific environmental conditions (Britto and Kronzucker, 2013). These preferences for different forms of N are influenced by the requirement for distinct uptake systems for NH_4^+ or NO_3^-, with significant consequences for plant-induced modifications of the rhizosphere (Britto and Kronzucker, 2002; Britto and Kronzucker, 2005). As an indispensable constituent of multiple organic molecules, such as nucleic acids, proteins, and chlorophyll, N plays a pivotal role in plant metabolism. The assimilation of the different N forms takes place via distinct metabolic pathways that interact in different ways with carbon metabolism and affect the composition of plant tissues (Krapp, 2015).

While many aspects of N nutrition in the context of plant development have been extensively investigated, the effect on cell wall biosynthesis, composition, and assembly remains poorly understood. Plant cell walls are complex networks constructed by a load-bearing framework of cellulose microfibrils,

Abbreviations:AIR, alcohol-insoluble residue; AX, arabinoxylan; CoMPP, comprehensive microarray polymer profiling; DM, degree of methylesterification; FA, ferulic acid; HG, homogalacturonan; MLG, mixed linkage glucan.

embedded and cross-linked within a matrix of hemicelluloses, pectins, structural proteins, and, in specific cells, lignin (secondary cell walls) (Cosgrove, 2005). Except for the protein parts of proteoglycans, most cell wall components lack N *per se*. However, this element is essential for primary metabolism and consequently cell wall biosynthesis. Several cases of species-specific and dose-dependent effects of plant N status on the construction of the cell wall network have already been reported (Allison *et al.*, 2012; Gutiérrez-Rodríguez *et al.*, 2013; Camargo *et al.*, 2014; Baldwin *et al.*, 2017). N deficiency not only inhibits plant growth and development but also leads to distinct changes in cell walls, including decreased cellulose but increased xyloglucan content and rearrangement of pectin (Fernandes et al., 2013, 2016a, b). Transcriptomic analyses have revealed that high and low affinity nitrate transporters are co-expressed with a range of cell wall remodelling genes, namely those participating in the synthesis of pectin, xyloglucans, and cellulose (Landi and Esposito, 2017). On the other hand, ammonium transporters in *Arabidopsis thaliana* showed very limited connection with enzymes involved in cell wall synthesis (Podgórska *et al.*, 2017). Nevertheless, distinct cell wall remodelling processes leading to increased cell wall rigidity in Arabidopsis plants utilizing NH_4^+ as the sole N source have also been observed (Podgórska *et al.*, 2017). The majority of evidence supporting cell wall modifications triggered by N form come from plants that possess type I cell walls. Unfortunately, less is known about the effects of different inorganic N sources on the composition of grass-specific type II cell walls. Members of the Poaceae (grasses and cereals) are globally important crops providing food and feed, and, more recently, biomass feedstocks for biorefining.

In the present study, we used the *Brachypodium distachyon* inbred line Bd21-3 representing a model for commelinid monocot plant species, which has been extensively used over the past decades to better understand various aspects of grass biology and biomass utilization (Draper *et al.*, 2001; Bevan *et al.*, 2010; Vain, 2011; Scholthof *et al.*, 2018). Like other members of the grass family, *B. distachyon* responds to N fertilization by increasing its growth rate and yield (Barhoumi, 2017).

Our aim was to investigate the response of *B. distachyon* cell walls to different inorganic N sources (NH_4NO_3, NO_3^-, or NH_4^+). To gain insights into the composition of major groups of cell wall building components and associated three-dimensional architectures, we combined quantitative chemical analyses with comprehensive microarray polymer profiling (CoMPP). We established that different types of N source inflicted a wide range of alterations in the composition and assembly of plant cell walls in an organ- and time-dependent manner.

Materials and methods

Plant material and growth conditions

Seeds of *B. distachyon* (inbred line Bd21-3) wild-type plants were surface sterilized as described by Alves *et al.* (2009). Briefly, the seeds were soaked in ultrapure water (Milli-Q Element, Merck) and washed in 70% (v/v) ethanol followed by 1.3% sodium hypochlorite (v/v). Thereafter, the seeds were thoroughly rinsed with sterile ultrapure water and vernalized in the dark at 5 °C for 4 d. The seeds were then placed on pieces of Grodan (Grodan, Roermond, The Netherlands) in bottom-cut 1.5 ml microcentrifuge tubes. First, to ensure uniform growth, seeds were pre-germinated by placing the tubes containing seeds in 1 mM $CaSO_4$ for a period of 3 weeks in a climate chamber at 18/20 °C (day/night) and 16 h photoperiod. After 3 weeks, seedlings were supplied every 4 d with fresh nutrient solution containing 2 mM $MgSO_4$, 0.1 mM KH_2PO_4, 0.1 mM Na_2SiO_3, 50 μM NaFe(III)-EDTA, 50 μM H_3BO_3, 5 μM $MnCl_2$, 5 μM $ZnSO_4$, 0.5 μM $CuSO_4$, 0.1 μM Na_2MoO_3, and 5 mM MES pH 5.5. N was supplied as three distinct sources: (i) mixed N medium (NH_4NO_3): 1.25 mM $Ca(NO_3)_2$, 2.5 mM K_2SO_4, 0.75 mM $CaSO_4$, and 1.25 mM $(NH_4)_2SO_4$; (ii) nitrate medium (NO_3^-): 1 mM KNO_3, 2 mM $Ca(NO_3)_2$, and 2 mM K_2SO_4; and (iii) ammonium medium (NH_4^+): 2.5 mM K_2SO_4, 2 mM $CaSO_4$, and 2.5 mM $(NH_4)_2SO_4$, and provided together with the other nutrients. The plants were harvested at three developmental stages corresponding to the Biologische Bundesanstalt, Bundessortenamt und CHemische Industrie (BBCH) scale developmental stages of tillering (BBCH 20–29), heading (BBCH 51–59), and senescence (BBCH 89–92) (Hong *et al.*, 2011). At each stage, plants were separated into shoots and roots. Roots were blotted dry with paper tissue prior to weighing. In addition, at the heading stage, the plants were subdivided into (i) leaf blades and sheaths; (ii) stems; and (iii) spikelets (flowers, seeds, and bracts). At senescence (maturity), plants were separated into the straw (leaves with sheaths and stems) and spikelets. The material was collected in the following replicas: (i) three pools of 17 plants at the tillering stage; (ii) three pools of four plants at the heading stage; and (iii) three pools of three plants at senescence. Harvested material was frozen in liquid nitrogen and stored in −80 °C prior to further analysis. The experiment was repeated twice, in each case with at least three replicates per treatment.

Determination of total element concentrations

Shoots from the plants subjected to different N sources, harvested, and subdivided at the three distinctive growth stages, were dried at 60 °C for 3 d and pulverized by shaking with a zirconium ball in a mixer mill (MM400, Retsch, Haan, Germany). Subsequently, the plant material (100 mg) was digested by acid hydrolysis as described in Baldwin *et al.* (2017). The elemental composition of the samples was measured by inductively coupled plasma optical emission spectrometry (ICP-OES; Agilent 5100, Agilent Technologies, Manchester, UK). Reference material (spinach leaf, NCS ZC73013, China National Analysis Center for Iron and Steel, Beijing, China) was included in the analysis.

Determination of nitrogen concentrations

All the harvested and subdivided plant material, dried and pulverized as previously described, was weighed into tin capsules. N concentrations were analysed by Dumas combustion using a Vario Macro cube elemental analyser (Elementar Analysensysteme GmbH, Hanau, Germany). Data quality was evaluated by analysis of standard reference materials [1515 Apple leaves and 141d acetanilide, National Institute of Standards and Technology (NIST), Gaithersburg, MD, USA].

Preparation of alcohol-insoluble residue

Alcohol-insoluble residue (AIR) was prepared following Fry (1988), with adaptations. Fresh shoots from the plants subjected to the different N forms, harvested at the three time points and subdivided, were ground in liquid N and washed with 70% (v/v) ethanol, followed by 100% acetone; the remaining pellet (AIR) was left to air-dry. Starch was removed enzymatically as described by Fleischer *et al.* (1999). The AIR was suspended in 100 mM potassium phosphate, pH 6.8, and digested with α-amylase (0.5 U mg^{-1} AIR, α-amylase from *Bacillus subtilis* Type II A, SIGMA A6814-1MU) for 24 h at room temperature. The pellet was washed thoroughly with water and 100% acetone, and freeze-dried.

Crystalline cellulose concentration

The concentration of crystalline cellulose was determined in all the harvested shoot samples as described previously by Foster *et al.* (2010), based

on the method reported by Updegraff (1969). De-starched AIR was incubated in 2 M trifluoroacetic acid (TFA) at 121 °C for 90 min. The released glucose was quantified using the colorimetric anthrone assay, and the absorbance was measured at 625 nm in a microplate reader (Eon™ High Performance Microplate Spectrophotometer, BioTek) against a standard curve prepared with glucose. The anthrone assay was performed in three technical replicates for each sample.

Quantification of acetyl bromide-soluble lignin

The concentration of acetyl bromide-soluble lignin (ABSL) was determined in all the harvested shoot samples according to the method of Hatfield *et al.* (1999). The concentration of ABSL was calculated from the UV absorbance at 280 nm (Eon™ High Performance Microplate Spectrophotometer, BioTek) using a molar extinction coefficient of 18.126 g^{-1} l cm^{-1} (Fukushima and Hatfield, 2004) and a path length of 0.6345 cm. Quantification of ABSL was performed in triplicate for each sample.

Compositional analysis of non-cellulosic polysaccharides

The composition of non-cellulosic polysaccharides was determined according to Foster *et al.* (2010) with modifications. Due to shortage of plant material, analysis was performed only for samples harvested at the heading stage and maturity. De-starched AIR material (5 mg) was hydrolysed in 2 M TFA for 90 min at 121 °C. TFA was removed by drying under vaccum. TFA breaks down the cell wall network to release primarily non-cellulosic polysaccharides, and some fractions of cellulose that contain kinks and chain dislocations (amorphous form). The composition of monosaccharides in the filtrate was determined and quantified by high-performance anion-exchange chromatography coupled with integrated pulsed amperometric detection (HPAEC-iPAD) using Thermo Scientific Dionex ICS5000 as described previously by Głazowska *et al.* (2018). The system was calibrated with standards (L-Ara, D-Xyl, D-Gal, D-Glc, D-GlcA, and D-GalA) (Sigma). All calculations were done in Chromeleon CDS software.

Quantification of mixed linkage glucans

The content of mixed linkage glucans (MLGs) was determined by the mixed linkage β-glucan assay kit (Megazyme; Wicklow, Ireland) based on the specific release of β-D-(1,3;1,4)-glucan oligomers after enzymatic digestion with lichenase, followed by hydrolysis with β-glucosidase. Released D-Glc was then quantified using a glucose oxidase/peroxidase reagent. Ground barley and oat flour, provided by the manufacturer, served as reference material. The protocol was adapted to 5 mg of AIR, and all the subsequent reaction volumes were reduced 10-fold compared with the manufacturer's instructions. The concentration of MLGs was determined in triplicate for each sample.

Determination of the degree of methylesterification of galacturonic acid

The degree of methylesterification (DM) was determined in aerial samples harvested at the heading stage and maturity, according to the modified alcohol oxidase method of Klavons and Bennett (1986) and Lionetti *et al.* (2015). De-starched AIR (4 mg) was saponified for 1 h at room temperature by suspending in 0.25 M NaOH. The solution was then neutralized with HCl and centrifuged. The supernatant containing methanol and alcohol oxidase (0.05 U in 0.1 M sodium phosphate, pH 7.5; Sigma) was loaded into a microplate and incubated for 20 min at room temperature with shaking. Then, a mixture containing 0.02 M 2,4-pentanedione in 2 M ammonium acetate and 0.05 M acetic acid was added to each well, and incubated for an additional 10 min at 68 °C. Samples were cooled down on ice and the absorbance measured at 412 nm in a microplate reader (Eon™ High Performance Microplate Spectrophotometer, BioTek). The DM was calculated as the molar ratio of methanol to GalA (expressed as a percentage). The content of GalA was quantified previously by HPAEC-PAD, as described above.

Comprehensive microarray polymer profiling (CoMPP)

The analysis was performed essentially according to the method reported by Moller *et al.* (2007) and Zhang *et al.* (2014). Briefly, 10 mg of AIR was used for sequential extraction with 50 mM *trans*-1,2-diaminocyclohexane-*N*,*N*,*N*′,*N*′-tetraacetic acid (CDTA), pH 7.5, followed by 4 M NaOH containing 0.1% (v/v) $NaBH_4$. Each extraction was performed in triplicate, and pooled to one sample. Each sample was printed onto the same sheet of a nitrocellulose membrane, with three technical replicates and three 5-fold dilutions giving eight spots per sample. The arrays were incubated with the primary monoclonal antibodies (mAbs) listed in Supplementary Table S1 at *JXB* online and summarized by Rydahl *et al.* (2018). After washing with phosphate-buffered saline (PBS), arrays were probed with secondary antibodies conjugated with alkaline phosphatase. Arrays were washed and developed using a 5-bromo-4-chloro-3-indolyl-phosphate (BCIP)/nitro-blue tetrazolium chloride (NBT) substrate and scanned using a flatbed scanner (CanoScan 9000 Mark II, Canon, Søborg, Denmark) at 2400 dpi.

Each spot on the array was converted to a value based on pixel intensity as described by Moller *et al.* (2007). The average of the nine values representing a sample (three technical replicates, three dilutions each) was calculated and served as the basis of one number in the heatmap. The highest signal in the data set was set to 100, and all other values were normalized accordingly to the highest value as indicated by the colour scale bar.

Enzymatic treatment and labelling with xylan-directed probes

The arrays prepared previously were labelled with an additional set of antibodies specific for xylans, namely LM27, LM28, INRA-AX, and INRA-UX (Supplementary Table S1). In addition, prior to the labelling, some arrays were subjected to enzymatic treatment with a solution containing 5 U of α-L-arabinofuranosidase from *Aspergillus niger* (Megazyme), which removes α-(1,2)- and α-(1,3)-linked arabinofuranose (Ara*f*) residues. The incubation was carried out as described by the manufacturer. Briefly, the arrays were incubated for 30 min in 100 mM sodium acetate buffer, pH 4 at 40 °C. Control non-treated arrays were incubated for an equivalent time with the corresponding buffers. Immunolabelling of the arrays and signal quantification were performed as previously described.

Immunolocalization and phloroglucinol staining

Approximately 1 cm long pieces cut from the middle of the second internode (counting from the top) were sampled at the heading stage from plants receiving the three different N sources. Sections, 100 µm thick, were prepared and analysed as described by Baldwin *et al.* (2017). Briefly, the sections were incubated with the primary antibody (LM12, PlantProbes), washed with PBS, and incubated with anti-rat secondary antibody conjugated to AlexaFluor555 (Invitrogen). Finally, the sections were washed and mounted on a glass slide in CITIFLUOR (Agar Scientific) mounting media. The sections were scanned using a Leica SP5 confocal laser scanning microscope (CLSM) equipped with a UV diode (405 nm), and Ar (488 nm) and HeNe (543 nm) lasers. All sections were scanned with the same settings. For each treatment, a control slide was prepared following the description above without the initial incubation with the primary antibody. The control was used to check for unspecific binding of the secondary antibody to the cell walls.

To visualize lignin using Wiesner staining, a saturated solution of phloroglucinol (Sigma) in 20% HCl was prepared. The sections (prepared as described above) were placed in a drop of solution, incubated for ~5 min, and directly observed under an Olympus BX41 light microscope

Results

The source of N affects biomass production and morphology of roots and shoots

Throughout the growth cycle, NH_4NO_3 and NO_3^- supply had a similar effect on shoot development (Fig. 1). However,

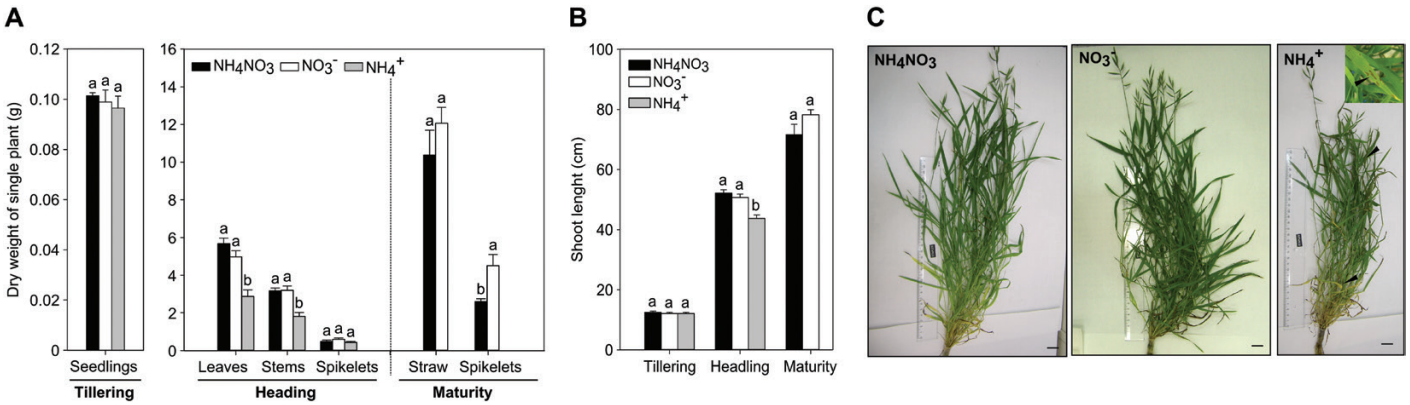

Fig. 1. The effect of N source on the shoot morphology. The weight of aerial parts of the wild-type plants (A), as well as the plant height (B), were measured at the three growth stages. Statistical comparisons were made using one-way ANOVA followed by Tukey's HSD post-hoc test; the letters indicate significant differences between the treatments within a given organ (mean ±SE, $n \geq 5$, $P<0.05$). Differences in shoot morphology were visible at the heading stage (C); the plants supplied with NH_4^+ grew less, had lesions on leaves, as well as chlorosis and wilting of leaves, as indicated by arrowheads. Scale bars=2 cm.

at maturity, NO_3^--treated plants had an almost 2-fold higher yield of spikelets than NH_4NO_3-fed plants (Fig. 1A). Long-term application of only NH_4^+ resulted in a reduction of shoot height and dry weight of leaves and stems at the heading stage, and the plants developed significantly shorter and less abundant leaves (Fig. 1; Supplementary Table S2). Over time, plants utilizing NH_4^+ as the sole N source started to exhibit lesions on leaf blades, chlorosis of older leaves, general wilting, and increased susceptibility to fungal infection (Fig. 1C). Thus, the plant material from the NH_4^+-only treatment was not included in the sampling at maturity.

At the tillering stage, the relative weight of the root system was 30% higher for plants with access to only NO_3^- (Fig. 2A). At later stages, however, the difference in the root biomass between NH_4NO_3 and NO_3^- disappeared, whereas prolonged NH_4^+ supply resulted in a significant reduction of the fresh weight of the root system (Fig. 2A). In addition, when compared with the other N sources, plants utilizing NH_4NO_3 developed a significantly shorter primary root, as observed at the heading stage and onwards (Fig. 2B, D). Initially, root architecture was similar between the treatments, while at the heading stage application of only NH_4^+ or only NO_3^- had contrasting effects: NH_4^+ resulted in development of lateral root buds and short lateral roots (<1 mm), whilst NO_3^- was associated with elongation of lateral and crown roots (Fig. 2C). The root system of the plants grown with the mixed N source resembled that of the plants grown with only NO_3^- (Fig. 2C, D).

Different inorganic N forms affect total N concentration in shoots as well as concentration and partitioning of other micro- and macroelements

The use of the different N sources was reflected in changes in the total N concentration in the aerial tissues. Initially, plants growing on NO_3^- medium exhibited the lowest N concentration, while at the heading stage, the N concentration in all sampled organs was similar in plants supplied with NO_3^- or NH_4NO_3 (Fig. 3). In contrast, at the same stage, plants supplied with NH_4^+ had a higher N concentration in spikelets and a lower concentration in leaves compared with the other treatments (Fig. 3). Differences between the NH_4NO_3 and NO_3^- treatments emerged at maturity, where the NH_4NO_3 supply yielded 27% and 19% higher N concentration in the straw and the spikelets, respectively (Fig. 3).

As expected, *B. distachyon* plants supplied with different sources of inorganic N had significantly different elemental profiles, and the degree of alterations varied with growth stage and between the organs (Supplementary Figs S1, S2). Elements such as P, Fe, and Cu showed little sensitivity to the N supply, as the concentrations in shoots were similar in most of the samples (Supplementary Figs S1, S2). In contrast, the concentrations of K, Na, and Mn differed significantly between the treatments in all the samples (Supplementary Figs S1, S2).

Cell walls of plants utilizing NO_3^- as the sole N source are high in crystalline cellulose at early growth stages and low in lignin at the heading stage

The results described above show that different N sources influence the growth and morphology of *B. distachyon* plants as well as their uptake of mineral elements. We therefore hypothesized that the composition of cell walls could also be affected. To test that, we first quantified the content of crystalline cellulose and lignin.

Significant differences in the relative amount of crystalline cellulose between the treatments were only present in growth stages before, but not at, maturity (Fig. 4A). Plants supplied with NO_3^- as the sole N source contained the relatively highest amount of crystalline cellulose at the tillering stage as well as in leaves during heading ($P<0.05$; Fig. 4A). In addition, at the heading stage, spikelets of plants receiving NO_3^- or NH_4^+ had a comparable amount of crystalline cellulose, ~15% higher than in the mixed treatment (Fig. 4A).

Differences in ABSL were most pronounced at the heading stage, where the NO_3^--fed plants exhibited a >20% reduction in the concentration of ABSL across all tested organs relative to the other N treatments (Fig. 4B). At maturity, the lignin concentration in the spikelets differed significantly, being 14% lower in the plants

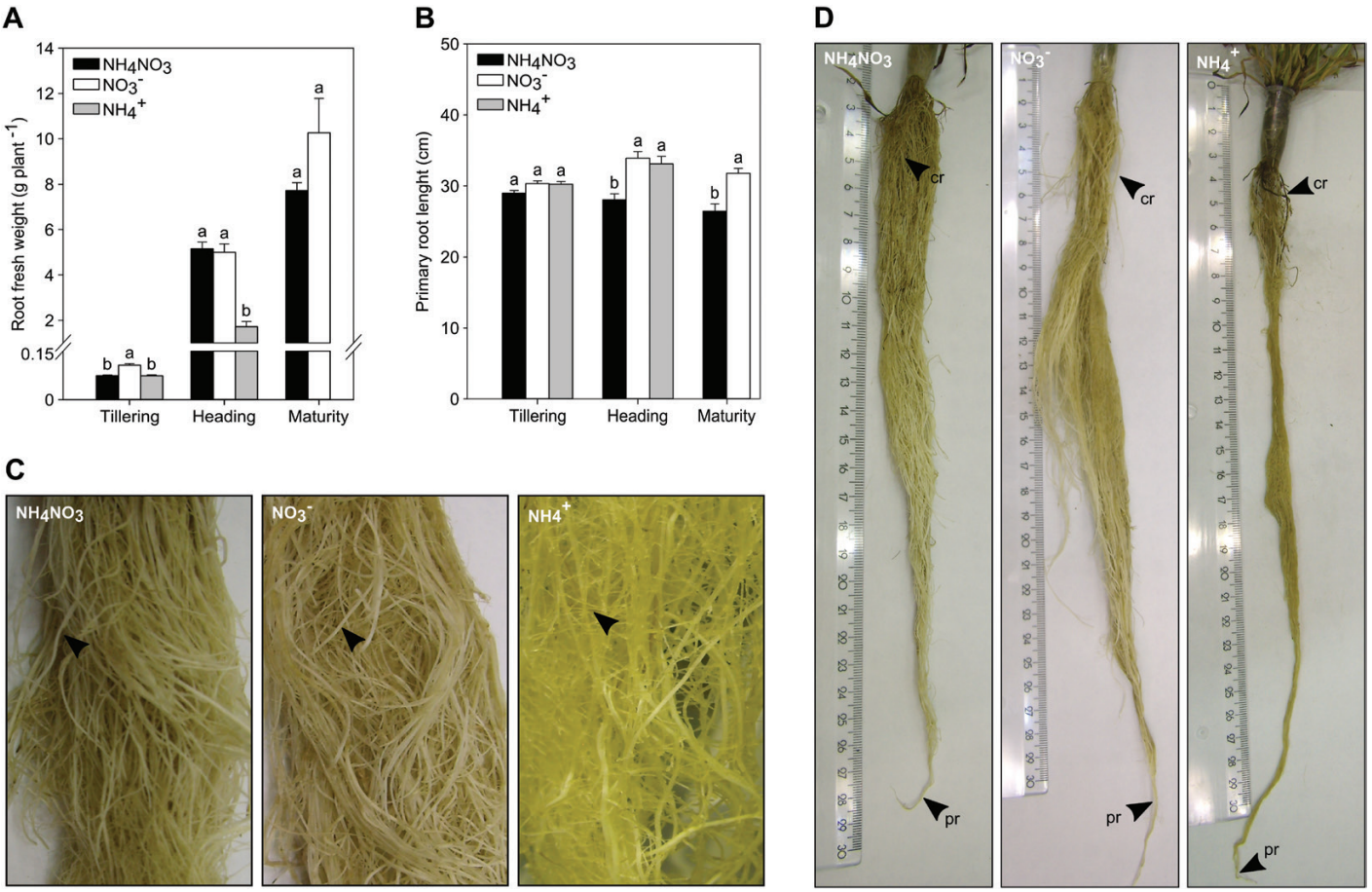

Fig. 2. The source of inorganic N distinctly affects root system architecture of *Brachypodium distachyon*. Relative fresh weight of the root system (A) and length of the primary root (B) of the wild-type plants (accession Bd21-3) were measured at three developmental stages: tillering, heading, and senescence. Different letters indicate significant differences between the treatments within the given organ (mean ±SE, $n \geq 5$) as assessed by one-way ANOVA followed by Tukey's HSD post-hoc test ($P<0.05$). At the heading stage, differences in formation of lateral and crown roots were visible between the treatments as indicated by arrowheads (C). At the same growth stage, different N forms also modulated the architecture of the whole root system, including variation in primary root length, and in abundance of crown roots and lateral roots (D). cr, crown roots; pr; primary roots.

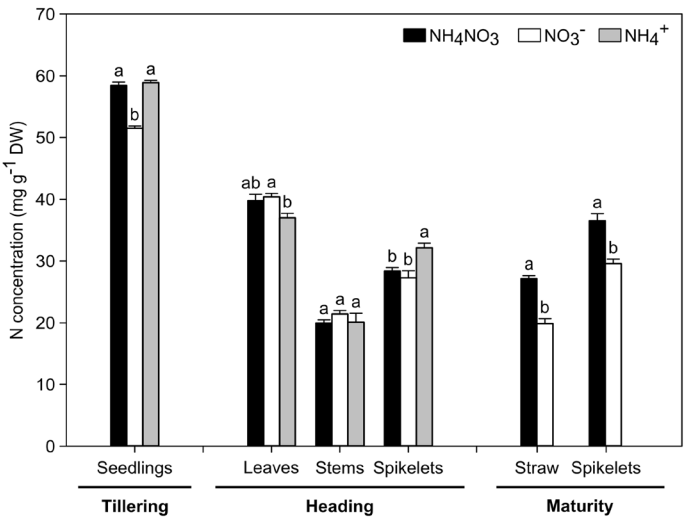

Fig. 3. The concentration of total N in aerial tissues of the plants varies with the form of N applied and with the developmental stage. N concentration in above-ground plant parts was measured by Dumas combustion. All measurements were taken at three stages of development: tillering, heading, and maturity. Mean values (±SE) are presented ($n \geq 3$). Different letters indicate significant differences between the treatments within a given organ ($P<0.05$); statistical comparisons were made using one-way ANOVA followed by Tukey's HSD post-hoc test.

grown on NO_3^- compared with the mixed N treatment (Fig. 4B). Histochemical Wiesner staining of *B. distachyon* stems at the heading stage was consistent with the chemical quantification of lignin (Fig. 4B, C). In the plants supplied with NH_4NO_3 or NH_4^+, lignin polymers were detected in the inner and outer vascular bundles, bundle sheaths, and in interfascicular fibres (Fig. 4C). The intensity of lignin staining in the plants supplied with NO_3^- was significantly reduced in comparison with that in the NH_4NO_3 and NH_4^+ treatments (Fig. 4C).

Sole NO_3^- supply results in the lowest degree of methylesterification of HG at the heading stage, while NH_4^+ and NO_3^- supply leads to increased GalA concentration in leaves

To assess potential changes in cell wall composition in response to different N forms, we performed detailed analysis of non-cellulosic polysaccharides using CoMPP (Fig. 5). CoMPP analysis is a semi-quantitative immunomicroarray-based method that provides a profile of extractable cell wall polysaccharides released in two consecutive extractions, first with CDTA, followed by NaOH. Since differences in cell wall architecture, particularly the way in which the polymers are linked, may have a strong effect on extractability of certain epitopes, we

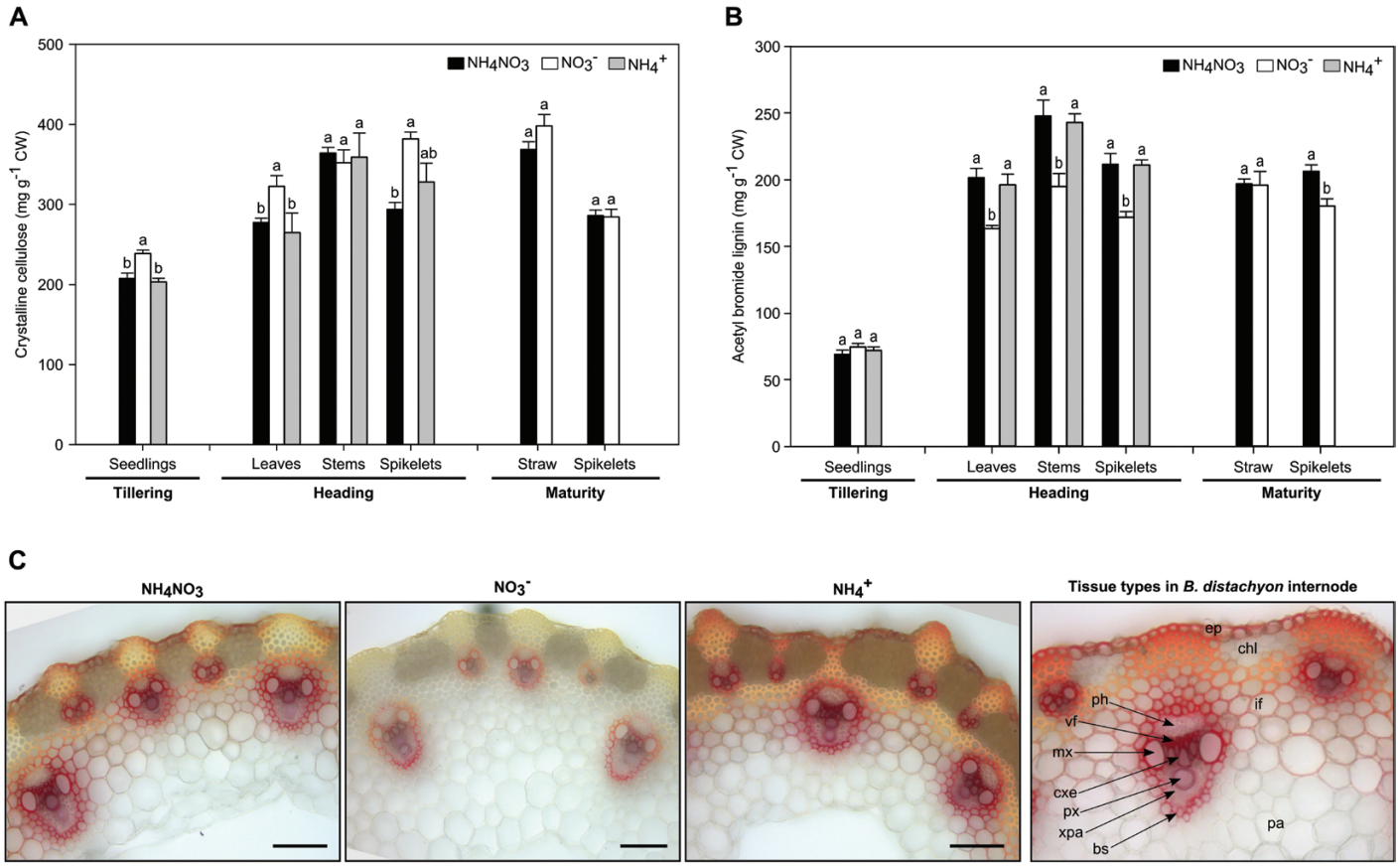

Fig. 4. *Brachypodium distachyon* plants show alterations in concentrations of crystalline cellulose and acetyl bromide-soluble lignin. Quantifications of crystalline cellulose (A) and acetyl bromide-soluble lignin (B) were carried out with wild-type *B. distachyon* B21-3 plants harvested at tillering, heading, and maturity growth stages. Mean values (±SE) are presented ($n \geq 6$). Different letters indicate significant differences between the treatments within a given organ ($P<0.05$) as assessed by one-way ANOVA followed by Tukey's HSD post-hoc test. Distribution of lignin in stem sections sampled at the heading stage was compared using histochemical Wiesner staining (phluoroglucinol) (C). Scale bar=50 µm. bs, bundle sheath; chl, chlorenchyma; cxe, connecting xylem elements; ep, epidermis; if, interfascicular fibres; mx, metaxylem; pa, parenchyma; ph, phloem; px, protoxylem; vf, vascular fibres; xpa, xylem parenchyma.

performed additional quantification of the monosaccharide composition of non-cellulosic polysaccharides (pectin and hemicelluloses) released with TFA (Table 1). Only samples harvested at the heading stage and at maturity were included in the analysis, as the amount of material harvested at the tillering stage was not sufficient.

Pectin accounts for a minor fraction of the cell walls in grasses, with homogalacturonan (HG) being the most abundant pectin constituent. HG consists of a linear backbone of (1,4)-linked α-D-GalA residues, commonly partly methylesterified at C-6 (Mohnen, 2008). Epitopes characteristic for HG with a different degree and pattern of methylesterification were mostly present in the CDTA-extracted fraction (Fig. 5A, B). The most striking differences between the treatments were observed in the spikelets (Fig. 5A). At the heading stage, the plants supplied with only NO_3^- showed the lowest signal for mAbs recognizing de-esterified HG (Fig. 5A). At maturity, the opposite pattern was observed, namely lower values in the NH_4NO_3 compared with the NO_3^- treatment (Fig. 5A). GalA reached the highest concentration in the leaves at the heading stage, where the differences between the treatments were the most prominent (Table 1). The plants supplied with NO_3^- and NH_4^+ had a comparable concentration of GalA in leaves, and the values were 36% and 25% higher ($P<0.05$), respectively, than for the mixed treatment (Table 1). Finally, the DM of GalA was assessed. At the heading stage, the NO_3^- supply resulted in the lowest DM in all the analysed organs (Fig. 6). DM in the leaves was 18% and 29% lower ($P<0.05$) in the NH_4^+ and NO_3^- treatments compared with NH_4NO_3 (Fig. 6). At senescence, the DM of spikelet samples was almost 2-fold higher than at the heading stage, but there were no differences between the N treatments, while in the mature straw of NO_3^--supplied plants, the DM was 21% higher ($P<0.05$) than in the straw of the NH_4NO_3-supplied plants (Fig. 6). The quantitative data characterizing HG mostly did not correspond to the patterns observed on CoMPP, thus indicating that in this context the heatmap provides information on HG extractability and consequently architectural rearrangements, rather than abundance *per se*.

NH_4^+ supply causes enhanced MLG deposition in all organs at the heading stage, whereas NO_3^- supply has the opposite effect at maturity

Epitopes characteristic for hemicelluloses were primarily released in the NaOH fraction (Fig. 5B). Structures detected

A CDTA fraction

		Tillering			Heading									Maturity			
		Seedlings			Leaves			Stems			Spikelets			Straw		Spikelets	
		NH_4NO_3	NO_3^-	NH_4^+	NH_4NO_3	NO_3^-	NH_4^+	NH_4NO_3	NO_3^-	NH_4^+	NH_4NO_3	NO_3^-	NH_4^+	NH_4NO_3	NO_3^-	NH_4NO_3	NO_3^-
HG	HG partially/de-esterified **(JIM5)**	23	23	21	32	29	31	6	8	7	24	15	18	26	27	15	25
HG	HG partially esterified **(JIM7)**	13	16	12	41	36	36	7	11	8	22	20	21	22	19	33	38
HG	HG partially/de-esterified **(LM18)**	25	32	30	39	34	35	6	9	0	24	17	23	31	35	18	27
HG	HG partially/de-esterified **(LM19)**	30	37	30	34	28	29	0	0	0	21	10	20	26	30	12	24
RG-I	RG-1 backbone **(INRA-RU1)**	9	10	11	0	0	0	0	0	0	6	6	6	0	0	10	11
RG-I	(1→4)-β-D-galactan **(LM5)**	0	0	0	7	0	6	0	9	8	9	11	11	0	0	13	14
RG-I	(1→5)- α-arabinan **(LM6)**	16	20	21	26	16	27	14	18	19	21	25	26	28	26	31	30
RG-I	Linearised (1→5)-α-arabinan **(LM13)**	0	0	0	0	0	0	0	0	0	0	0	0	0	0	8	7
FA	Feruloylate on any polymer **(LM12)**	15	14	17	26	16	26	22	23	26	44	51	46	22	21	48	54
MLG	MLG **(BS-400-3)**	0	7	5	10	6	10	0	6	8	15	13	18	7	0	42	41
XG	Xyloglucan **(LM25)**	0	0	0	8	0	9	7	6	10	0	7	6	8	7	8	10
Xylan	(1→4)-β-D-xylan **(LM10)**	0	0	0	0	0	0	0	0	0	8	10	6	0	0	0	0
Xylan	(1→4)-β-D-xylan/ AX **(LM11)**	0	0	0	8	0	7	9	8	9	54	62	57	0	0	36	32
Proteoglycans	Extensin **(LM1)**	0	0	0	5	0	0	0	6	0	7	6	0	6	6	0	0
Proteoglycans	Extensin **(JIM20)**	10	15	12	16	6	15	7	19	18	15	20	14	21	19	16	14
Proteoglycans	AGP **(JIM13)**	11	18	14	20	11	18	16	29	22	23	28	16	25	23	29	26
Proteoglycans	AGP **(LM14)**	0	6	4	6	0	6	0	7	7	9	8	0	5	6	0	0
Proteoglycans	AGP, β-linked GlcA **(LM2)**	11	20	14	14	7	15	0	10	9	13	17	8	13	12	14	13

B NaOH fraction

		Tillering			Heading									Maturity			
		Seedlings			Leaves			Stems			Spikelets			Straw		Spikelets	
		NH_4NO_3	NO_3^-	NH_4^+	NH_4NO_3	NO_3^-	NH_4^+	NH_4NO_3	NO_3^-	NH_4^+	NH_4NO_3	NO_3^-	NH_4^+	NH_4NO_3	NO_3^-	NH_4NO_3	NO_3^-
HG	HG partially/de-esterified **(LM18)**	6	0	0	0	0	0	0	0	0	0	0	6	0	0	0	0
HG	HG partially/ de-esterified **(LM19)**	14	14	13	13	14	14	9	12	12	17	17	20	18	15	16	15
RG-I	RG-1 backbone **(INRA-RU1)**	36	34	36	39	39	38	31	36	36	39	42	42	44	39	37	34
RG-I	(1→4)-β-D-galactan **(LM5)**	15	15	17	24	27	22	41	45	48	33	37	34	38	32	29	28
RG-I	(1→5)- α-arabinan **(LM6)**	49	48	47	52	51	58	39	42	48	46	44	54	59	54	47	43
RG-I	Linearised (1→5)-α-arabinan **(LM13)**	8	9	10	21	20	29	15	17	27	29	31	37	28	21	28	27
MLG	MLG **(BS-400-3)**	58	57	56	66	66	67	81	83	87	64	67	67	74	66	83	91
XG	Xyloglucan (XXXG) **(LM15)**	22	15	17	27	33	26	27	31	28	35	41	38	34	33	21	19
XG	Xyloglucan **(LM25)**	45	42	43	48	47	43	57	59	64	42	45	46	58	52	46	42
Xylan	(1→4)-β-D-xylan **(LM10)**	22	26	27	43	51	46	81	79	86	89	90	96	68	50	74	68
Xylan	(1→4)-β-D-xylan/ AX **(LM11)**	44	48	48	56	63	54	76	75	74	82	82	86	69	63	69	75
Proteoglycans	Extensin **(JIM20)**	8	8	8	8	9	7	10	11	9	6	7	0	6	6	0	0
Proteoglycans	AGP **(JIM13)**	12	13	13	22	24	22	30	34	35	24	25	23	30	29	29	24
Proteoglycans	AGP, β-linked GlcA **(LM2)**	0	0	0	7	9	7	9	12	12	9	9	10	13	12	10	9

0 100

Fig. 5. Composition of CDTA- and NaOH-extractable fractions of *B. distachyon* plants is affected by the source of available N. Plants were harvested at three growth stages, subdivided as previously described, and subjected to extraction with CDTA (A) followed by NaOH. (B) The values presented are average signal intensities ($n \geq 4$), and the colour intensity is correlated with the signal strength; white corresponds to low and red to high intensity. The names of antibodies and the epitopes they recognize are indicated along the *y*-axis. Antibodies that did not show a signal for all the samples are not included in the heatmap, but are listed in Supplementary Table S1. HG, homogalacturonan; RG-I, rhamnogalacturonan I; FA, ferulic acid; MLG, mixed linkage glucan; XG, xyloglucan; AX, arabinoxylan; AGP, arabinogalactan protein; GlcA, glucuronic acid.

with CoMPP can be classified into three types of hemicelluloses, namely xylans, MLGs, and xyloglucans. MLGs consists of β-D-(1,3)- and β-D-(1,4)-linked glucosyl residues, and are particularly abundant in young plants and seeds of *B. distachyon*. TFA-released Glc in *B. distachyon* primarily originates from both MLGs and regions of non-crystalline amorphous cellulose, and to a lesser extent from xyloglucans (Table 1). At the heading stage, the Glc concentration in the leaves was 17% and 20% lower ($P<0.05$) in the solely NO_3^--supplied plants than in the plants receiving NH_4NO_3 or NH_4^+, respectively (Table 1). Conversely, in mature spikelets, NO_3^- supply resulted in a 24% higher glucose concentration compared with the NH_4NO_3 supply (Table 1). To assess whether MLGs are the source of glucose alterations, the concentrations of the polymer in the

Table 1. *Profile of monosaccharides released by TFA hydrolysis of non-cellulosic polysaccharides from wild-type* B. distachyon *supplied with different N forms*

Harvest	Organ	N form	Xyl	Glc	Ara	Gal	GalA	GlcA	Ara/Xyl
Heading	Leaves	NH_4NO_3	143±4 a	**48±2 a**	36±1 a	8.6±0.4 a	7.9±0.25 b	4.0±0.13 b	0.28±0.004 b
		NO_3^-	142±5 a	40±1 b	41±1 a	8.6±0.3 a	**9.9±0.33 a**	4.0±0.10 b	**0.30±0.004 a**
		NH_4^+	146±7 a	**50±3 a**	38±2 a	8.6±0.4 a	**10.7±0.34 a**	**4.8±0.14 a**	0.28±0.003 b
	Stems	NH_4NO_3	202±7 a	45±2 a	35±1 a	6.9±0.4 a	6.6±0.22 a	2.6±0. 07 b	0.17±0.002 b
		NO_3^-	190±3 a	44±1 a	35±1 a	7.1±0.1 a	7.0±0.30 a	**3.1±0.07 a**	**0.18±0.001 a**
		NH_4^+	201±3 a	44±2 a	37±1 a	7.1±0.3 a	7.6±0.41 a	**3.3±0.10 a**	**0.18±0.001 a**
	Spikelets	NH_4NO_3	197±7 b	34±2 a	33±1 c	6.1±0.4 a	6.5±0.29 a	2.6±0.08 a	0.17±0.002 b
		NO_3^-	210±5 ab	34±2 a	**38±1 b**	6.4±0.2 a	7.2±0.23 a	2.7±0.11 a	**0.18±0.002 a**
		NH_4^+	**229±8 a**	32±2 a	**42±1 a**	7.0±0.3 a	6.5±0.33 a	2.8±0.10 a	0.18±0.004 ab
Maturity	Straw	NH_4NO_3	187±6 a	36±3 a	42±1 a	9.5±0.2 b	8.5±0.36 a	4.0±0.13 a	0.23±0,006 b
		NO_3^-	170±8 a	35±3 a	44±1 a	**10.5±0.3 a**	7.8±0.34 a	4.1±0.19 a	**0.26±0.010 a**
	Spikelets	NH_4NO_3	**180±4 a**	**86±4 a**	**35±1 a**	**5.5±0.1 a**	2.7±0.17 b	2.0±0.15 a	0.20±0.005 b
		NO_3^-	145±5 b	107±3 b	31±1 b	5.0±0.2 b	**3.5±0.32 a**	2.3±0.14 a	**0.21±0.003 a**

Neutral sugars and uronic acids were separated and quantified by high-performance anion-exchange chromatography with pulsed amperometric detection (HPAEC-PAD). All measurements were taken at two sampling times: heading and maturity. The Ara/Xyl ratio of TFA-extractable arabinoxylans was calculated using the corresponding Ara and Xyl concentrations presented in this table. Data represents means ±SE and $n \geq 6$. Different letters indicate significant differences between the treatments within the given organ ($P<0.05$) as assessed by one-way ANOVA followed by Tukey's HSD post-hoc test. Concentrations are given in μg mg^{-1} cell wall. Data in bold are statistically significant differences between the treatments.

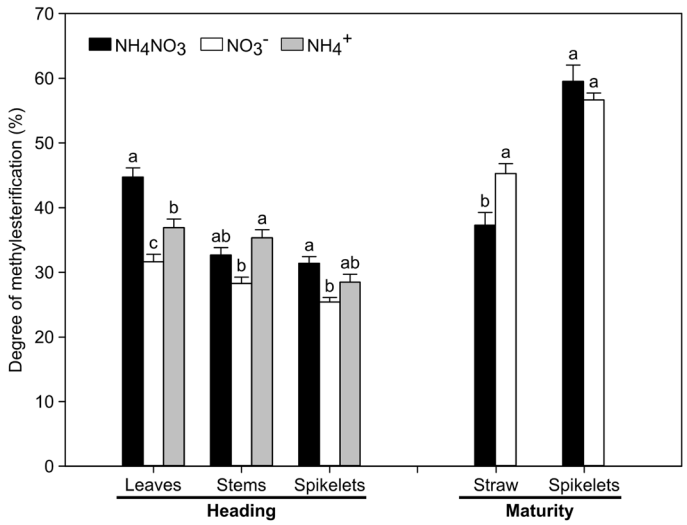

Fig. 6. The degree of methylesterification (DM) of non-cellulosic polysaccharides varies between treatments and organs. The DM of GalA (%) represents the molecular ratio of methanol to GalA released by TFA. Data represents means ±SE ($n \geq 6$). Different letters indicate statistically significant differences between the treatments within a given organ ($P<0.05$) as assessed by one-way ANOVA followed by Tukey's HSD post-hoc test.

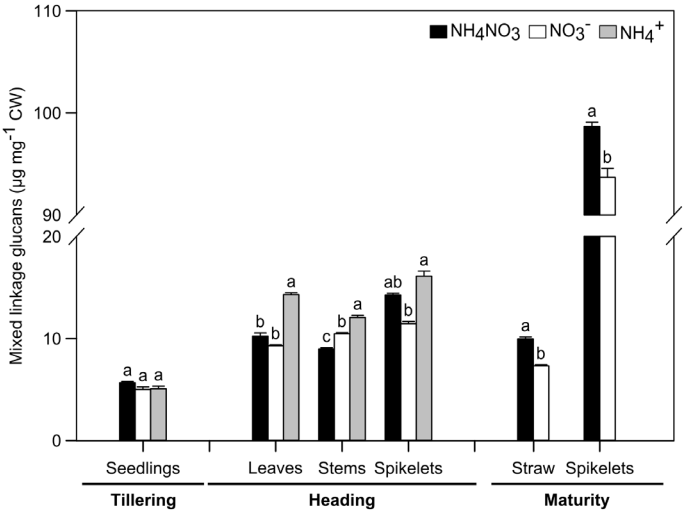

Fig. 7. The concentration of mixed linkage glucans (MLGs) in *Brachypodium distachyon* plants supplied with different N forms. The MLG concentrations in the samples were quantified with the lichenase-based enzymatic assay. Mean values (±SE) are presented ($n \geq 3$). Different letters indicate significant differences between the treatments within a given organ ($P<0.05$) as assessed by one-way ANOVA followed by Tukey's HSD post-hoc test.

samples were determined using a specific lichenase-based enzymatic assay. In the plants supplied with NH_4^+, the MLG concentration in all the vegetative organs was significantly higher compared with the plants receiving the other N sources (Fig. 7). In the spikelets of NH_4^+-treated plants, the MLG concentration was higher ($P<0.05$) than that in the plants receiving NO_3^- only (Fig. 7). At maturity, the concentration of MLGs in the spikelets was >7-fold higher than at the heading stage (Fig. 7). In addition, the concentration of MLG in the straw and spikelets was >36% and 5% higher, respectively, in plants supplied with NH_4NO_3 than with NO_3^- only (Fig. 7). The MLGs quantified with the enzymatic assay did not corroborate changes in Glc concentration, thus indicating amorphous cellulose or/and xyloglucan as the source of alterations (Table 1). The MLGs accounted for ~20–30% of the Glc released with TFA from the vegetative organs at the heading stage (leaves and stems) and maturity (straw) (Supplementary Table S3). A much larger proportion of Glc released by TFA treatment of the spikelets seemed to be originating from MLGs, namely 34–50% at the heading stage and >87% at maturity (Supplementary Table S3).

Characterization of arabinoxylans

Xylans are the most abundant hemicellulose in grasses; the xylan backbone is substituted with α-L-(1,2) or α-L-(1,3)-linked Ara*f* and ester-liked hydroxycinnamates (Scheller and Ulvskov, 2010). Additionally, grass-type xylan may carry α-(1,2)-GlcA substitutions (Scheller and Ulvskov, 2010). The relative abundance of xylan in the samples was detected with LM10 antibody binding to the Xyl backbone and LM11 that recognizes both unsubstituted xylans and regions substituted with Ara*f*. Alterations of xylan epitopes between the treatments were mostly detected in the NaOH fraction (Fig. 5). At the heading stage, leaves of the plants supplied with NO_3^- were characterized by higher occurrence of both xylan epitopes as compared with the other N sources (Fig. 5B). At the same stage, the NH_4^+ nutrition resulted in the highest abundance of xylan epitopes in spikelets (LM10 and LM11) and stems (LM10) among the N treatments (Fig. 5B). At maturity, the plants supplied with NH_4NO_3 showed substantially higher abundance of LM10 and LM11 epitopes in the straw samples, while in the spikelets a similar pattern was true for LM10, but not for LM11, which was substantially lower than in the plants supplied with NO_3^- (Fig. 5B).

Significant differences in Ara and Xyl concentrations were observed only in the spikelets at both growth stages (Table 1). At the heading stage, the NH_4^+ treatment resulted in a substantially higher concentration of Xyl ($P<0.05$) than the mixed N treatment (Table 1). The Ara concentration differed significantly among all the treatments, being highest with NH_4^+ supply and lowest with NH_4NO_3 (Table 1). These observations corresponded well with the higher abundance of LM10 and LM11 epitopes (Fig. 5B). At maturity, the concentration of xylose and arabinose in the spikelets of plants supplied only with NO_3^- were 19% and 10% lower than in the corresponding spikelets of the NH_4NO_3-fed plants (Table 1). GlcA showed the highest concentrations in the leaves at the heading stage, where the differences between the treatments were the most prominent (Table 1). Plants supplied solely with NH_4^+ had >20% higher concentrations of GlcA in the leaves compared with the other treatments (Table 1). In the stems, mixed N treatment resulted in a significantly lower GlcA concentration compared with only NO_3^- or NH_4^+ (Table 1).

We believe that the highest portion of TFA-extractable Ara and Xyl originates from the breakdown of arabinoxylans (AXs). Thus, the Ara/Xyl ratio might serve as a rough estimate of xylan backbone substitution. Plants supplied with the NO_3^- were characterized by the highest Ara/Xyl ratio among all the treatments; the values were slightly, but significantly, different from those observed in all analysed organs of plants in the NH_4NO_3 treatment and in the leaves from the NH_4^+ treatment (Table 1). Alterations in the quantity of Ara and Xyl, and the accompanying changes in the abundance of xylan and AX epitopes, indicate modifications of the xylan fraction. To verify that, we included an additional set of xylan-directed antibodies recognizing various substitution patterns and we combined it with directed hydrolysis of those substitutions using arabinofuranosidase (Fig. 8A; Supplementary Fig. S3). Enzymatic removal of Ara*f* substitution did not affect the strength of signal for LM10, except for stem and spikelet samples at the heading stage, where it led to overall increased intensity (Supplementary Fig. S3). On the other hand, the enzyme treatment resulted in decreased or completely absent LM11 signal in all the samples, which confirms that LM11 recognized primarily AXs (Supplementary Fig. S3). The only exception was the spikelet fraction at the heading stage, which was unaffected by the enzymatic digestion (Supplementary Fig. S3). The INRA-AX antibody, similar to LM10, recognizes mostly unsubstituted xylan backbones. As for LM10, the INRA-AX epitopes were primarily present in the NaOH fraction and showed a similar intensity pattern upon N treatment to that observed for LM10 (Figs 5B, 8A). LM27 was shown to bind strongly to heteroxylans from grass cell walls. In our study, the LM27 signal, similar to that of LM11, was present in both the extracted fractions and was substantially lower in the leaf sample of plants treated with NO_3^- compared with the other treatments (Fig. 8A). Finally, LM28 and INRA-UX, which have been shown to bind to glucuronosyl-containing epitopes in heteroxylans, exhibited no differences in response to different N forms (Fig. 8A). Digestion with arabinofuranosidase had a distinct effect on the xylan-directed antibody signal intensities, no binding of LM28 and INRA-AX, and strongly reduced binding of LM27 in the CDTA fraction (Fig. 8A). Despite the overall trend of a decrease in the signal in the NaOH fraction upon enzymatic treatment, LM27 showed higher binding in the spikelets at maturity and INRA-UX in stems at the heading stage (Fig. 8A). Arabinofuranosidase action further enhanced differences between the N treatments in the NaOH fraction probed with LM28 and INRA-AX (Fig. 8A).

In *B. distachyon*, Ara*f* residues of AXs can be further substituted with molecules of ferulic acid (FA). In our study, the extraction with CDTA was successful in releasing some polysaccharides containing FA based on the LM12-generated signal (Fig. 5A). Compared with the other N treatments, NO_3^- as sole N source resulted in significantly lower abundance of epitopes recognized by the LM12 antibody in leaves at the heading stage (Fig. 5A). Modification of adjacent AXs with FA may lead to cross-linking of the molecules and further bridging of the hemicelluloses with lignin, consequently affecting the mechanical properties of cell walls (Buanafina, 2009). To further explore the differences observed with CoMPP, we performed immunolocalization using the LM12 antibody on stem cross-sections sampled at the heading stage (Fig. 8B). The distribution of the LM12 signal in the stems sampled from plants supplied with NH_4NO_3 or NO_3^- was comparable (Fig. 8B), showing a strong fluorescence signal in the lignified interfascicular fibres, the polar sclerenchyma, and some parenchymatic cells adjacent to the pit (Fig. 8B). In contrast, the LM12 signal was much weaker when NH_4^+ was the sole N source and was only observed in the parenchyma cells contiguous with the pit (Fig. 8B).

Discussion

Growth and morphology of B. distachyon *and consequences for mineral nutrition*

Plants can utilize inorganic N present alone as either NO_3^- or NH_4^+; however, the preferred form depends, among other factors, on the plant species, soil characteristics, and N availability (Britto and Kronzucker, 2013). In this study, application

A Xylan-directed labelling

			Tillering			Heading									Maturity			
			Seedlings			Leaves			Stems			Spikelets			Straw		Spikelets	
			NH_4NO_3	NO_3^-	NH_4^+	NH_4NO_3	NO_3^-	NH_4^+	NH_4NO_3	NO_3^-	NH_4^+	NH_4NO_3	NO_3^-	NH_4^+	NH_4NO_3	NO_3^-	NH_4NO_3	NO_3^-
LM27	CDTA	Non-treated	3	4	4	19	11	24	9	14	13	27	29	29	15	16	41	44
		Arabinofuranosidase	1	2	2	14	7	18	4	6	7	23	26	27	10	10	39	41
	NaOH	Non-treated	21	23	22	28	28	25	20	23	24	30	28	32	31	30	35	37
		Arabinofuranosidase	11	16	14	22	22	24	11	16	16	29	30	33	29	25	40	42
LM28	CDTA	Non-treated	6	7	10	9	5	10	8	10	13	17	20	22	7	9	20	19
		Arabinofuranosidase	0	0	0	0	0	0	0	0	0	1	2	2	0	0	2	3
	NaOH	Non-treated	36	36	37	39	41	38	59	58	63	42	46	46	53	51	47	48
		Arabinofuranosidase	23	23	26	30	32	29	30	39	40	32	35	38	39	33	31	29
INRA-AX	CDTA	Non-treated	2	2	2	3	1	3	1	4	4	13	22	21	2	2	15	13
		Arabinofuranosidase	0	0	0	0	0	0	0	0	0	0	0	0	0	0	0	0
	NaOH	Non-treated	41	42	45	50	58	50	71	75	76	82	85	87	67	61	75	73
		Arabinofuranosidase	16	17	22	27	30	24	54	64	65	79	85	79	40	24	47	36
INRA-UX	CDTA	Non-treated	0	0	0	0	0	0	0	0	0	0	0	0	0	0	0	0
		Arabinofuranosidase	0	0	0	0	0	0	0	0	0	0	0	0	0	0	0	0
	NaOH	Non-treated	3	5	5	7	7	5	6	9	10	5	5	8	11	10	6	5
		Arabinofuranosidase	1	1	1	2	2	2	33	38	43	16	21	13	12	5	9	4

0 100

B LM12

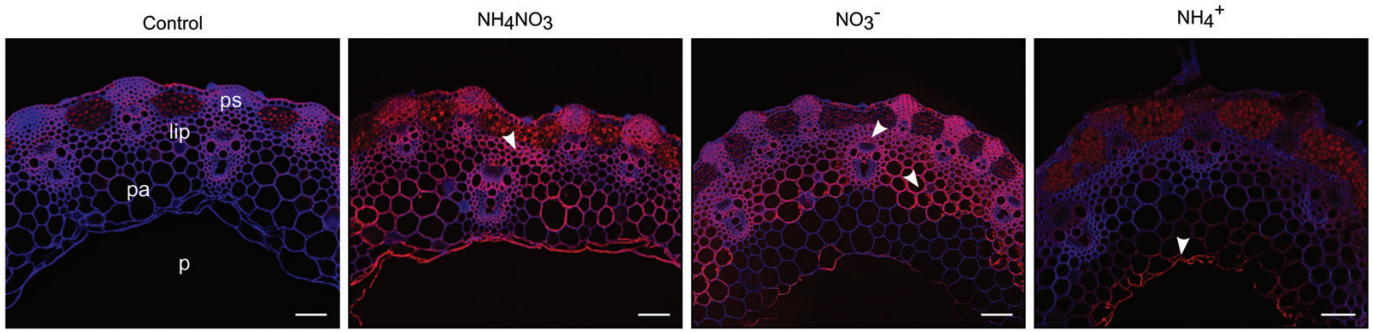

Fig. 8. Characterization of arabinoxylan epitopes upon supply with different N forms. (A) On-array treatment with arabinofuranosidase was performed to assess removal of xylan arabinose side chains using antibodies LM27, LM28, INRA-AX, and INRA-UX with different specificity for xylan substitutions. Plants were harvested at the three developmental stages of growth, subdivided as previously described, and subjected to extraction with CDTA followed by NaOH. The values presented are average signal intensities ($n \geq 4$), and the colour is correlated with the signal strength; white corresponds to low and red to high intensity. The names of antibodies and the epitopes they recognize are indicated along the *y*-axis. (B) The presence of feruloylated polysaccharides in sections of internodes collected at the heading stage was detected with LM12 mAb. Images are overlays of the emission from Calcofluor White (blue signal) counterstain outlining the cell walls and antibody labelling (red signal). Arrowheads indicate strongly labelled lignified interfascicular fibres and pith parenchyma. Unspecific interaction of anti-rat secondary antibody with the cell wall was tested for all the treatments; the results were comparable among the treatments and are depicted in the control image. Scale bars=50 μm. lip, lignified interfascicular parenchyma; pa, parenchyma; ps, polar sclerenchyma; p, pit.

of NO_3^-, either as the sole N source or together with NH_4^+, strongly promoted biomass production of *B. distachyon* (line Bd21-3) plants (Fig. 1; Supplementary Table S2). Conversely, plants receiving only NH_4^+ developed symptoms previously reported as indicative of ammonium toxicity (Britto and Kronzucker, 2002; Podgórska *et al.*, 2017). In addition, different inorganic N sources strongly affected the root architecture in *B. distachyon* (Fig. 2). A similar response to NO_3^- and NH_4^+ application was previously also observed in *A. thaliana*, where the complementary effect of the two N forms on lateral root development was suggested as an adaptive trait to utilize available N efficiently (Remans *et al.*, 2006; Lima *et al.*, 2010). NH_4^+ and NO_3^- account for a substantial proportion of the ions taken up by plants, and the concentration of N in shoot dry matter (Fig. 3) is relatively high compared with most other essential plant nutrients. The availability and consequently the uptake of different N forms results in alterations in the acquisition of other mineral nutrients, reflecting changes inflicted on cation–anion balance and pH regulation (Carlisle *et al.*, 2012; Hawkesford *et al.*, 2012). Overall, *B. distachyon* plants supplied with NO_3^- as the sole N source tended to have a higher concentration of cations in shoots compared with the plants receiving only

NH_4^+ (Supplementary Figs S1, S2). This pattern matches that observed in several other plant species (Britto and Kronzucker, 2002; Roosta and Schjoerring, 2007).

The form of inorganic nitrogen supplied causes distinct cell wall remodelling patterns

The porous organization of the polymers within the cell wall network enables communication of the cell with the extracellular environment, while at the same time giving shape to the cell and protecting it from harmful factors. Thus, in order to carry out those multiple roles efficiently, cell walls have an ability to remodel and reinforce their structure and/or composition when biosynthesis or deposition into the network of a given component is impaired (Wolf *et al.*, 2012). Recent studies reported distinct remodelling of type I cell walls of *A. thaliana* in response to NO_3^- and NH_4^+ (Landi and Esposito, 2017; Podgórska *et al.*, 2017). We hypothesize that similar modulation is triggered in *B. distachyon* possesing type II cell walls.

Cellulose and lignin

Models of cellulose assembly in plants state that the fibrils form both crystalline (ordered) and amorphous (dislocated/less ordered) regions. Comparing the different N treatments, plants supplied solely with NO_3^- had the highest crystalline cellulose concentration in shoots at the tillering stage and in leaves at the heading stage (Fig. 4A). This observation supports previously reported co-expression of NO_3^- transporters and cellulose synthase genes in *A. thaliana* (Landi and Esposito, 2017) and might indicate alteration of the fibril arrangement in the network. At the same time, lignin concentrations at the heading stage of plants supplied only with NO_3^- were significantly reduced (Fig. 4B). A similar observation in tobacco and rice was explained by NO_3^-- and NO_2^--mediated inhibition of the phenylpropanoid pathway, resulting in reduced levels of phenylpropanoids and consequently decreased lignin deposition (Fritz *et al.*, 2006; Wang *et al.*, 2014). Lack of changes in lignin concentration in the mature straw (Fig. 4B) corresponds well with previous reports of reduced NO_3^- uptake at the flowering stage (Rossato *et al.*, 2001; Masclaux-Daubresse *et al.*, 2010). In such a case, the tissue levels of NO_3^- might become insufficient to inhibit the phenylpropanoid pathway, hence resulting in a similar lignin concentration between the treatments at maturity (Fig. 4B).

Non-cellulosic polysaccharides

Despite a relatively low abundance in grasses, pectins play important structural roles as modifications of their structure have widespread effects on the properties of the cell wall (Wolf and Greiner, 2012). The architecture of HG, namely the degree and pattern of distribution of methyl groups along the HG backbone, affects the adhesive capacity of HG, the resistance to degradation, and the rheological properties of the cell wall matrix (Caffall and Mohnen, 2009; Lionetti *et al*, 2010). The form of supplied N appeared to have a strong effect on the biosynthesis and remodelling of HG, particularly at the heading stage, which represent the vital transition between the vegetative and generative phase (Figs 5A, 6). Supply of only NO_3^- led to a significantly lower DM in all the organs at the heading stage (Fig. 6). De-methylesterification of pectin has been linked with both cell wall softening and stiffening, depending on different actions of pectin methylesterases (PMEs) (Willats *et al.*, 2001*b*, 2006). The blockwise de-esterification of pectins, mediated by PMEs, favours cell wall stiffening via formation of Ca^{2+} bridges between de-methylesterified regions (>9) of neighbouring HG chains (Wolf and Greiner, 2012). In contrast, non-blockwise PME action leads to scattered de-methylesterification along the HG chains, resulting in regions that less effectively form Ca^{2+} cross-links. This may increase cell wall porosity and enable the action of enzymes leading to cell wall loosening and/or degradation (Willats *et al.*, 2001*a*). Thus, lower signals for several antibodies recognizing HGs in leaves and spikelets of the plants supplied with only NO_3^- (Fig. 5), despite the higher or comparable pectin concentrations (Table 1), indicate blockwise de-methylesterification resulting in cell wall stiffening which results in reduced extractability. As the plants matured, the DM in the straw of plants supplied with only NO_3^- was relatively high (Fig. 6). As plants mature, the deposition of lignin increases and the higher methylesterification status might be necessary to provide a porous structure for lignin deposition.

In type II cell walls the hemicelluloses are far more abundant than pectins, comprising mainly AXs and MLGs (Carpita, 1996; Smith and Harris, 1999). MLGs have been suggested to participate in the organization of cellulose fibrils and in interactions with AXs, thus playing a key structural role by preventing aggregation of microfibrils (Smith-Moritz *et al.*, 2015; Martínez-Sanz *et al.*, 2017). High concentrations of MLGs are present in the endosperm cell walls of *B. distachyon* and were assumed to contribute to the storage polysaccharide pool (Guillon *et al.*, 2011). Plants supplied with NH_4^+ as a sole N source had a relatively high MLG concentration in all the organs at the heading stage, while the opposite was the case in mature spikelets and straw of plants receiving only NO_3^- (Fig. 7), strongly indicating a role for N in regulation of MLG biosynthesis. It is unclear whether N directly regulates the process or if the changes rather reflect a compensatory cell wall rearrangement. A wide range of growth stage-specific and treatment-dependent alterations in the AX fraction observed in our work highlights the complexity of the interaction between N metabolism and cell wall biosynthesis. FA-mediated cross-linking of adjacent AXs and interaction with lignin substantially strengthens the structure of the cell wall (de Oliveira *et al.*, 2015). Plants supplied with NH_4NO_3 or NO_3^- alone grew significantly taller, produced more biomass, and differed significantly with respect to the extractability of AXs, the deposition of lignin, and FA than the plants receiving only NH_4^+ (Figs 2, 5, 8). The degree and pattern of distribution of the backbone substituents strongly affect the properties of xylans and determine the nature and extent of the interactions with cellulose and lignin, consequently affecting cell wall recalcitrance (Wu *et al.*, 2013; Smith *et al.*, 2017). Thus, the N form supplied to *B. distachyon* has a dual effect, affecting the level of xylans (Table 1; Figs 5B, 8A) and their substitutions, resulting in differences in the chemical and enzymatic extractability of AX epitopes (Figs 5, 8A).

Conclusions

Brachypodium distachyon plants respond to different inorganic N forms by changing their root and shoot morphology along with biomass production. Despite the fact that N is not a constituent of the most abundant cell wall polymers, the range of alterations in composition and assembly of plant cell walls in both an organ-specific and a time-dependent manner can be linked to different N sources. Cell walls of plants supplied with NO_3^- as the sole N source tend to have a relatively high cellulose content and a low lignin content at the heading stage. In contrast, NO_3^- supply results in reduced methylesterification of HGs at the heading stage and modification of the structure of AXs, particularly in the spikelets. On the other hand, at the heading stage, NH_4^+ supply is associated with high lignin and MLG content in all the above-ground plant parts. The distinct cell wall remodelling observed throughout the development of *B. distachyon* supplied with different N forms suggests cross-talk between N metabolism and cell wall synthesis, involving a regulatory network that modulates the cell wall architecture to match the physiological processes accompanying uptake and assimilation of different N forms. The presented data further highlight the possibilities for tailoring the cell wall biomass through fine-tuning of N supply.

Supplementary data

Supplementary data are available at *JXB* online.

Table S1. Monoclonal antibodies used in this study.

Table S2. Morphological traits of *Brachypodium distachyon* shoots as affected by inorganic N source.

Table S3. Characterization of the origin of pools contributing to the glucose released from cell walls by TFA hydrolysis.

Fig, S1. Elemental composition of wild-type *Brachypodium distachyon* plants supplied with different N forms.

Fig. S2. Radar plots presenting multielemental profiles of plants supplied with different inorganic N sources.

Fig. S3. Characterization of arabinoxylan epitopes upon supply with different N forms.

Acknowledgements

We would like to thank Thomas H. Hansen, Lena Byrgesen, Anja Hecht Ivø, and Louise Nancke for their excellent technical assistance. The authors acknowledge the Center for Advanced Bioimaging (CAB) (University of Copenhagen, Denmark), for providing facility and equipment for sample preparation and collecting imaging data in this study. This work was supported by the Innovation Fund Denmark: grant number 001-2011-4 (B21st: Biomass for the 21st century) and grant number 12-132625 (Bio-Value). The authors declare that the research was conducted in the absence of any commercial or financial relationships that could be construed as a potential conflict of interest.

Author contribution

SG and JKS planned and designed the research; SG prepared samples for ICP-OES, CoMPP, HPAEC analysis, and CN determination, and performed the experimental work; JM performed immunolocalization and staining; ChB carried out HPAEC measurements; JUF processed the CoMPP data; SG wrote the manuscript and revised it together with LB, JM, and JKS; all authors have read and approved the final version.

References

Allison GG, Morris C, Lister SJ, Barraclough T, Yates N, Shield I, Donnison IS. 2012. Effect of nitrogen fertiliser application on cell wall composition in switchgrass and reed canary grass. Biomass and Bioenergy **40**, 19–26.

Alves SC, Worland B, Thole V, Snape JW, Bevan MW, Vain P. 2009. A protocol for *Agrobacterium*-mediated transformation of *Brachypodium distachyon* community standard line Bd21. Nature Protocols **4**, 638–649.

Baldwin L, Głazowska S, Mravec J, Fangel J, Zhang H, Felby C, Willats WG, Schjoerring JK. 2017. External nitrogen input affects pre- and post-harvest cell wall composition but not the enzymatic saccharification of wheat straw. Biomass and Bioenergy **98**, 70–79.

Barhoumi Z. 2017. Insights into the growth response and nitrogen accumulation and use efficiency of the Poaceae grass *Brachypodium distachyon* to high nitrogen availability. Russian Journal of Plant Physiology **64**, 839–844.

Bevan MW, Garvin DF, Vogel JP. 2010. *Brachypodium distachyon* genomics for sustainable food and fuel production. Current Opinion in Biotechnology **21**, 211–217.

Bloom AJ. 2015. The increasing importance of distinguishing among plant nitrogen sources. Current Opinion in Plant Biology **25**, 10–16.

Britto DT, Kronzucker HJ. 2002. NH_4^+ toxicity in higher plants: a critical review. Journal of Plant Physiology **159**, 567–584.

Britto DT, Kronzucker HJ. 2005. Nitrogen acquisition, PEP carboxylase, and cellular pH homeostasis: new views on old paradigms. Plant, Cell & Environment **28**, 1396–1409.

Britto DT, Kronzucker HJ. 2013. Ecological significance and complexity of N-source preference in plants. Annals of Botany **112**, 957–963.

Buanafina MMD. 2009. Feruloylation in grasses: current and future perspectives. Molecular Plant **2**, 861–872.

Caffall KH, Mohnen D. 2009. The structure, function, and biosynthesis of plant cell wall pectic polysaccharides. Carbohydrate Research **344**, 1879–1900.

Camargo EL, Nascimento LC, Soler M, *et al*. 2014. Contrasting nitrogen fertilization treatments impact xylem gene expression and secondary cell wall lignification in Eucalyptus. BMC Plant Biology **14**, 256.

Carlisle E, Myers S, Raboy V, Bloom A. 2012. The effects of inorganic nitrogen form and CO_2 concentration on wheat yield and nutrient accumulation and distribution. Frontiers in Plant Science **3**, 195.

Carpita NC. 1996. Structure and biogenesis of the cell walls of grasses. Annual Review of Plant Physiology and Plant Molecular Biology **47**, 445–476.

Cosgrove DJ. 2005. Growth of the plant cell wall. Nature Reviews. Molecular Cell Biology **6**, 850–861.

de Oliveira DM, Finger-Teixeira A, Mota TR, Salvador VH, Moreira-Vilar FC, Molinari HB, Mitchell RA, Marchiosi R, Ferrarese-Filho O, dos Santos WD. 2015. Ferulic acid: a key component in grass lignocellulose recalcitrance to hydrolysis. Plant Biotechnology Journal **13**, 1224–1232.

Draper J, Mur LA, Jenkins G, Ghosh-Biswas GC, Bablak P, Hasterok R, Routledge AP. 2001. *Brachypodium distachyon*. A new model system for functional genomics in grasses. Plant Physiology **127**, 1539–1555.

Fernandes JC, García-Angulo P, Goulao LF, Acebes JL, Amâncio S. 2013. Mineral stress affects the cell wall composition of grapevine (*Vitis vinifera* L.) callus. Plant Science **205–206**, 111–120.

Fernandes JC, Goulao LF, Amâncio S. 2016a. Immunolocalization of cell wall polymers in grapevine (*Vitis vinifera*) internodes under nitrogen, phosphorus or sulfur deficiency. Journal of Plant Research **129**, 1151–1163.

Fernandes JC, Goulao LF, Amâncio S. 2016b. Regulation of cell wall remodeling in grapevine (*Vitis vinifera* L.) callus under individual mineral stress deficiency. Journal of Plant Physiology **190**, 95–105.

Fleischer A, O'Neill MA, Ehwald R. 1999. The pore size of non-graminaceous plant cell walls is rapidly decreased by borate ester cross-linking of the pectic polysaccharide rhamnogalacturonan II. Plant Physiology **121**, 829–838.

Foster CE, Martin TM, Pauly M. 2010. Comprehensive compositional analysis of plant cell walls (lignocellulosic biomass) part II: carbohydrates. Journal of Visual Experiments **37**, pii: 1837. doi: 10.3791/1837.

Fritz C, Palacios-Rojas N, Feil R, Stitt M. 2006. Regulation of secondary metabolism by the carbon–nitrogen status in tobacco: nitrate inhibits large sectors of phenylpropanoid metabolism. The Plant Journal **46**, 533–548.

Fry SC. 1988. The growing plant cell wall: chemical and metabolic analysis. Essex, UK: Longman Scientific and Technical.

Fukushima RS, Hatfield RD. 2004. Comparison of the acetyl bromide spectrophotometric method with other analytical lignin methods for determining lignin concentration in forage samples. Journal of Agricultural and Food Chemistry **52**, 3713–3720.

Głazowska S, Baldwin L, Mravec J, *et al*. 2018. The impact of silicon on cell wall composition and enzymatic saccharification of *Brachypodium distachyon*. Biotechnology for Biofuels **11**, 171.

Guillon F, Bouchet B, Jamme F, Robert P, Quéméner B, Barron C, Larré C, Dumas P, Saulnier L. 2011. *Brachypodium distachyon* grain: characterization of endosperm cell walls. Journal of Experimental Botany **62**, 1001–1015.

Gutiérrez-Rodríguez E, Lieth HJ, Jernstedt JA, Labavitch JM, Suslow TV, Cantwell MI. 2013. Texture, composition and anatomy of spinach leaves in relation to nitrogen fertilization. Journal of the Science of Food and Agriculture **93**, 227–237.

Hatfield RD, Grabber J, Ralph J, Brei K. 1999. Using the acetyl bromide assay to determine lignin concentrations in herbaceous plants: some cautionary notes. Journal of Agricultural and Food Chemistry **47**, 628–632.

Hawkesford M, Horst W, Kichey T, Lambers H, Schjoerring JK, Moller IM, White P. 2012. Functions of macronutrients. In: Marschner P, ed. Marschner's mineral nutrition of higher plants, 3rd edn. San Diego: Elsevier Academic Press Inc., 135–189.

Hong SY, Park JH, Cho SH, Yang MS, Park CM. 2011. Phenological growth stages of *Brachypodium distachyon*: codification and description. Weed Research **51**, 612–620.

Klavons JA, Bennett RD. 1986. Determination of methanol using alcohol oxidase and its application to methyl ester content of pectins. Journal of Agricultural and Food Chemistry **34**, 597–599.

Krapp A. 2015. Plant nitrogen assimilation and its regulation: a complex puzzle with missing pieces. Current Opinion in Plant Biology **25**, 115–122.

Landi S, Esposito S. 2017. Nitrate uptake affects cell wall synthesis and modeling. Frontiers in Plant Science **8**, 1376.

Lima JE, Kojima S, Takahashi H, von Wirén N. 2010. Ammonium triggers lateral root branching in *Arabidopsis* in an AMMONIUM TRANSPORTER1;3-dependent manner. The Plant Cell **22**, 3621–3633.

Lionetti V, Francocci F, Ferrari S, Volpi C, Bellincampi D, Galletti R, D'Ovidio R, De Lorenzo G, Cervone F. 2010. Engineering the cell wall by reducing de-methyl-esterified homogalacturonan improves saccharification of plant tissues for bioconversion. Proceedings of the National Academy of Sciences, USA **107**, 616–621.

Lionetti V, Giancaspro A, Fabri E, Giove SL, Reem N, Zabotina OA, Blanco A, Gadaleta A, Bellincampi D. 2015. Cell wall traits as potential resources to improve resistance of durum wheat against *Fusarium graminearum*. BMC Plant Biology **15**, 6.

Martínez-Sanz M, Mikkelsen D, Flanagan BM, Gidley MJ, Gilbert EP. 2017. Multi-scale characterisation of deuterated cellulose composite hydrogels reveals evidence for different interaction mechanisms with arabinoxylan, mixed-linkage glucan and xyloglucan. Polymer **124**, 1–11.

Masclaux-Daubresse C, Daniel-Vedele F, Dechorgnat J, Chardon F, Gaufichon L, Suzuki A. 2010. Nitrogen uptake, assimilation and remobilization in plants: challenges for sustainable and productive agriculture. Annals of Botany **105**, 1141–1157.

Mohnen D. 2008. Pectin structure and biosynthesis. Current Opinion in Plant Biology **11**, 266–277.

Moller I, Sørensen I, Bernal AJ, *et al*. 2007. High-throughput mapping of cell-wall polymers within and between plants using novel microarrays. The Plant Journal **50**, 1118–1128.

Näsholm T, Kielland K, Ganeteg U. 2009. Uptake of organic nitrogen by plants. New Phytologist **182**, 31–48.

Podgórska A, Burian M, Gieczewska K, Ostaszewska-Bugajska M, Zebrowski J, Solecka D, Szal B. 2017. Altered cell wall plasticity can restrict plant growth under ammonium nutrition. Frontiers in Plant Science **8**, 1344.

Remans T, Nacry P, Pervent M, Filleur S, Diatloff E, Mounier E, Tillard P, Forde BG, Gojon A. 2006. The *Arabidopsis* NRT1.1 transporter participates in the signaling pathway triggering root colonization of nitrate-rich patches. Proceedings of the National Academy of Sciences, USA **103**, 19206–19211.

Roosta HR, Schjoerring JK. 2007. Effects of ammonium toxicity on nitrogen metabolism and elemental profile of cucumber plants. Journal of Plant Nutrition **30**, 1933–1951.

Rossato L, Lainé P, Ourry A. 2001. Nitrogen storage and remobilization in *Brassica napus* L. during the growth cycle: nitrogen fluxes within the plant and changes in soluble protein patterns. Journal of Experimental Botany **52**, 1655–1663.

Rydahl MG, Hansen AR, Kračun SK, Mravec J. 2018. Report on the current inventory of the toolbox for plant cell wall analysis: proteinaceous and small molecular probes. Frontiers in Plant Science **9**, 581.

Scheller HV, Ulvskov P. 2010. Hemicelluloses. Annual Review of Plant Biology **61**, 263–289.

Scholthof KBG, Irigoyen S, Catalan P, Mandadi KK. 2018. *Brachypodium*: a monocot grass model genus for plant biology. The Plant Cell **30**, 1673–1694.

Smith BG, Harris PJ. 1999. The polysaccharide composition of Poales cell walls: Poaceae cell walls are not unique. Biochemical Systematics and Ecology **27**, 33–53.

Smith PJ, Wang HT, York WS, Peña MJ, Urbanowicz BR. 2017. Designer biomass for next-generation biorefineries: leveraging recent insights into xylan structure and biosynthesis. Biotechnology for Biofuels **10**, 286.

Smith-Moritz AM, Hao Z, Fernández-Niño SG, *et al*. 2015. Structural characterization of a mixed-linkage glucan deficient mutant reveals alteration in cellulose microfibril orientation in rice coleoptile mesophyll cell walls. Frontiers in Plant Science **6**, 628.

Updegraff DM. 1969. Semimicro determination of cellulose in biological materials. Analytical Biochemistry **32**, 420–424.

Vain P. 2011. *Brachypodium* as a model system for grass research. Journal of Cereal Science **54**, 1–7.

Wang X, Li Y, Fang G, Zhao Q, Zeng Q, Li X, Gong H, Li Y. 2014. Nitrite promotes the growth and decreases the lignin content of *indica* rice calli: a comprehensive transcriptome analysis of nitrite-responsive genes during *in vitro* culture of rice. PLoS One **9**, e95105.

Willats WG, Orfila C, Limberg G, *et al*. 2001a. Modulation of the degree and pattern of methyl-esterification of pectic homogalacturonan in plant cell walls. Implications for pectin methyl esterase action, matrix properties, and cell adhesion. Journal of Biological Chemistry **276**, 19404–19413.

Willats WGT, Knox JP, Mikkelsen JD. 2006. Pectin: new insights into an old polymer are starting to gel. Trends in Food Science & Technology **17**, 97–104.

Willats WG, McCartney L, Mackie W, Knox JP. 2001b. Pectin: cell biology and prospects for functional analysis. Plant Molecular Biology **47**, 9–27.

Wolf S, Greiner S. 2012. Growth control by cell wall pectins. Protoplasma **249** Suppl 2, S169–S175.

Wolf S, Hématy K, Höfte H. 2012. Growth control and cell wall signaling in plants. Annual Review of Plant Biology **63**, 381–407.

Wu Z, Zhang M, Wang L, *et al*. 2013. Biomass digestibility is predominantly affected by three factors of wall polymer features distinctive in wheat accessions and rice mutants. Biotechnology for Biofuels **6**, 183.

Zhang H, Fangel JU, Willats WGT, Selig MJ, Lindedam J, Jørgensen H, Felby C. 2014. Assessment of leaf/stem ratio in wheat straw feedstock and impact on enzymatic conversion. GCB Bioenergy **6**, 90–96.